



Cite this: *Green Chem.*, 2015, **17**, 1744

## Mesoporous Zr-Beta zeolites prepared by a post-synthetic strategy as a robust Lewis acid catalyst for the ring-opening aminolysis of epoxides†

Bo Tang,<sup>a</sup> Weili Dai,<sup>a</sup> Xiaoming Sun,<sup>a,b</sup> Guangjun Wu,<sup>a</sup> Najia Guan,<sup>a</sup> Michael Hunger<sup>b</sup> and Landong Li\*<sup>a</sup>

Mesoporous zirconosilicate, stannosilicate, and titanosilicate with the BEA structure framework have been prepared from the commercially available Beta zeolite *via* acid–alkaline treatments and subsequent dry impregnation of appropriate organometallic precursors. N<sub>2</sub> adsorption–desorption isotherms and TEM observations confirm that alkaline treatment can induce desilication to create intra-crystalline mesopores from the partially dealuminated Beta sample. The incorporation of Zr species into the zeolite framework at formed silanol defect sites is monitored by infrared and <sup>1</sup>H MAS NMR spectroscopy. Characterization results from UV-vis and XPS reveal that the majority of the incorporated Zr species exist in the form of tetrahedral Zr(IV) in the zeolite framework. The creation of Lewis acid sites with moderate acid strength upon Zr incorporation is confirmed by FTIR spectroscopy with pyridine adsorption. The as-prepared mesoporous Zr-Beta exhibits a remarkable catalytic activity and regio-selectivity to β-amino alcohols in the ring-opening aminolysis of epoxides, and the presence of mesopores can promote the reaction to a great extent through enhanced mass transfer. The impacts of the Lewis acidity of the catalysts, the basicity of amines and adsorption of reactants on the ring-opening aminolysis of epoxides are discussed in detail.

Received 31st October 2014,  
Accepted 1st January 2015

DOI: 10.1039/c4gc02116a

www.rsc.org/greenchem

### 1. Introduction

Recently, heterogeneous Lewis acid materials, *e.g.* Ti-, Sn-, and Zr-Beta zeolites, have found widespread applications in sustainable chemistry and green chemical transformations.<sup>1–9</sup> Despite the attractive catalytic performance achieved, the exclusive presence of small micropores (typically 0.5–1 nm) in these microporous crystalline frameworks often imposes limited access and slow intra-crystalline diffusion of reactants and products, especially when dealing with bulky molecules in the liquid phase.<sup>10,11</sup> The low external surface area of the zeolite crystals is rapidly deactivated, which results in blockage of the micropores. With increasing academic and industrial interest in solid Lewis acid catalysts, feasible preparation strategies for solid Lewis acids without these drawbacks are urgently desired.

In the last decade, great attention has been paid to the exploitation of hierarchical/mesoporous metallosilicates,

which integrate the intrinsic microporosity with secondary inter- or intra-crystalline mesopores and accordingly increase the external surface area effectively. Meanwhile, the auxiliary pore structure brings about enhanced accessibility due to the enlarged pore mouths and shortened diffusion path in the micropores.<sup>11–13</sup> It can be expected that the use of a hierarchical/mesoporous zeolite instead of a conventional microporous zeolite may effectively improve the catalytic activity and reduce the catalyst deactivation.

Mesoporous Ti-zeolites and Sn-zeolites have been successfully prepared *via* bottom-up strategies and applied as catalysts in the epoxidation of olefins and Baeyer–Villiger oxidation reaction. For instance, Jinka *et al.*<sup>14</sup> reported the microwave-assisted synthesis of hierarchical Sn-MFI from a stannosilicate gel containing carbon particles as hard templates. Similar protocols were adopted by Ryoo *et al.*<sup>15</sup> and Román-Leshkov *et al.*<sup>16</sup> in the preparation of Ti-MFI and Sn-MFI nanosheets using a non-commercial organic structure directing agent. Very recently, Fan and co-workers<sup>17</sup> successfully synthesized a hierarchical Sn-MFI with ordered mesoporosity within the confined space of three dimensionally ordered mesoporous carbon by a seeded growth method, which exhibited a superior catalytic performance for the isomerization of cellulosic sugars. Nevertheless, the synthetic advantages of such bottom-up strategies are discounted by a low chance for large scale production, due to the use of costly and commercially unavailable

<sup>a</sup>Key Laboratory of Advanced Energy Materials Chemistry of Ministry of Education, Collaborative Innovation Center of Chemical Science and Engineering (Tianjin), Nankai University, Tianjin 300071, China. E-mail: lild@nankai.edu.cn; Fax: (+)86 22 23500341; Tel: (+)86 22 23500341

<sup>b</sup>Institute of Chemical Technology, University of Stuttgart, 70550 Stuttgart, Germany  
†Electronic supplementary information (ESI) available. See DOI: 10.1039/c4gc02116a

reactants as mesopore-inducing agents. Alternatively, post-synthetic modification offers an effective and versatile approach to many hierarchically structured zeolites.<sup>11,18–20</sup> Wu *et al.*<sup>21</sup> demonstrated that a remarkable catalytic performance could be achieved by the introduction of mesopores into the MOR crystals to improve the accessibility to Ti active sites by a post-synthetic strategy, *i.e.* alkaline treatment. Very recently, Pérez-Ramírez and co-workers have developed a simpler and more scalable alkaline-assisted metallation method to generate Lewis-acidic zeolites, which exhibited a remarkable performance in biomass conversion.<sup>22–24</sup> While desilication of aluminosilicates has been thoroughly explored, only a few studies have been reported on the desilication behavior of Beta zeolites in an alkaline solution.<sup>25–28</sup> On the basis of these issues, it is appealing to assess the potential for preparing mesoporous BEA-type zeolites containing metal ions *via* post-synthetic strategies and evaluating their catalytic performance as solid Lewis acids. It can be expected that the use of a hierarchical/mesoporous zeolite instead of a conventional microporous zeolite may effectively improve the catalytic activity and reduce the catalyst deactivation.

Ring-opening of epoxides with amines, *i.e.* aminolysis of epoxides, could lead to the formation of  $\beta$ -amino alcohols, which are used as versatile intermediates for the synthesis of various biologically active natural products, unnatural amino acids,  $\beta$ -blockers, insecticidal agents, chiral auxiliaries, and oxazolines.<sup>29–32</sup> As the most straightforward route to  $\beta$ -amino alcohols, several attempts have been made to realize the aminolysis of epoxides using homogeneous acid catalysts.<sup>33–36</sup> However, most of the homogeneous acid catalysts suffer from several disadvantages, *e.g.* separation issue, poor regio-selectivity, harsh reaction conditions, high dosage and cost of the catalyst, and the use of expensive or toxic solvents. Recently, solid Lewis acid catalysts, *i.e.* amorphous mesoporous titanosilicates and microporous TS-1, have been reported to be active and selective for the ring-opening of epoxides even at low temperatures and without a solvent.<sup>37–39</sup> Srivastava *et al.*<sup>40</sup> further reported that  $\beta$ -amino alcohols could be produced from aminolysis of epoxides with nanocrystalline Zr-MFI as the catalyst, demonstrating the potential of zirconosilicates in such a type of reaction.

In this work, BEA-type mesoporous zirconosilicate, stannosilicate, and titanosilicate are prepared *via* a post-synthesis strategy, including dealumination, desilication and Lewis acid site incorporation procedures. These materials are studied as catalysts for the ring-opening reaction of epoxides with amines to  $\beta$ -amino alcohols under ambient and solvent-free conditions. Mesoporous Zr-Beta zeolites exhibit a remarkable catalytic activity and regio-selectivity in epoxide aminolysis and the presence of mesopores could greatly promote the activity through enhanced mass transfer.

## 2. Experimental section

### 2.1 Zeolite materials

Commercial H-Beta with an  $n_{\text{Si}}/n_{\text{Al}}$  ratio of 16.7 (Nankai University) was used as the starting material for preparing Zr(IV)-

containing Beta catalysts with or without mesopores. Parent H-Beta was first treated with a 0.03 mol L<sup>-1</sup> oxalic acid solution (20 mL g<sup>-1</sup><sub>zeolite</sub>) at 343 K for 3 h. The slurry was filtered, thoroughly washed with deionized water, dried at 373 K overnight, and further calcined at 823 K for 5 h to obtain a partially dealuminated material with an  $n_{\text{Si}}/n_{\text{Al}}$  ratio of 22.4. Afterwards, alkaline treatment was performed on the partially dealuminated sample to generate mesopores. Briefly, 3 g of partially dealuminated H-Beta was dispersed in 60 mL of 0.2 mol L<sup>-1</sup> NaOH solution at 338 K for 0.5 h. The solid powder was filtered, washed with deionized water until the pH value was neutral, and then dried at 373 K overnight. The resulting sample was denoted as Meso-Beta with an  $n_{\text{Si}}/n_{\text{Al}}$  ratio of 15.8, which was subjected to acid treatment again with a 13 mol L<sup>-1</sup> nitric acid solution for 20 h to obtain siliceous Meso-Si-Beta ( $n_{\text{Si}}/n_{\text{Al}} > 1800$ ).

For reference, the parent H-Beta sample was directly refluxed with a 13 mol L<sup>-1</sup> nitric acid solution for 20 h to derive a siliceous microporous Beta sample, denoted as Si-Beta ( $n_{\text{Si}}/n_{\text{Al}} > 1800$ ).

### 2.2 Transition metal ion incorporation

Zr(IV)-containing microporous/mesoporous Beta materials were thus prepared using a simple and scalable post-synthetic strategy, *i.e.* the dry impregnation method, as reported in our previous work.<sup>41,42</sup> Before the incorporation of Zr, the Si-Beta or Meso-Si-Beta sample was pre-treated at 473 K overnight under vacuum to remove the physisorbed water. Afterwards, 1.0 g of the solid powder was finely ground with an appropriate amount of Cp<sub>2</sub>ZrCl<sub>2</sub> in the glovebox to achieve an intimate mixture with the  $n_{\text{Si}}/n_{\text{Zr}}$  ratio of 100. The solid mixture was then calcined under flowing air at 823 K for 6 h (heating rate at 5 K min<sup>-1</sup>) to derive the final zeolite, *i.e.* Zr-Beta and Meso-Zr-Beta.

For a better understanding of the active sites and the influence of mesopores on the catalytic activity, Ti(IV) and Sn(IV)-containing microporous/mesoporous Beta materials with a similar  $n_{\text{Si}}/n_{\text{M}}$  ratio (M = Ti or Sn) were also prepared. The preparation procedures are the same as those for Zr(IV)-containing Beta except that the organometallic precursors Cp<sub>2</sub>TiCl<sub>2</sub> and (CH<sub>3</sub>)<sub>2</sub>SnCl<sub>2</sub> were employed instead of Cp<sub>2</sub>ZrCl<sub>2</sub> for preparing Ti(IV)-containing and Sn(IV)-containing Beta, respectively.

### 2.3 Characterization techniques

X-ray diffraction (XRD) patterns of samples were recorded on a Bruker D8 diffractometer with CuK $\alpha$  radiation ( $\lambda = 1.54184 \text{ \AA}$ ) from 5° to 40° with a scan speed of  $2\theta = 6.0^\circ \text{ min}^{-1}$ .

The chemical compositions of the samples were determined by inductively coupled plasma atomic emission spectrometry (ICP-AES) on a Thermo IRIS Intrepid II XSP atomic emission spectrometer.

Diffuse reflectance infrared Fourier transform (DRIFT) spectra of the samples were measured on a Bruker Tensor 27 spectrometer with 128 scans at a resolution of 2 cm<sup>-1</sup>. A self-supporting pellet made of the sample material was placed in

the reaction chamber and pretreated in flowing dry air at 673 K for 1 h. The spectra were recorded in dry air against KBr as the background.

Fourier transform infrared (FTIR) spectra of pyridine adsorption were also collected on a Bruker Tensor 27 spectrometer. Self-supporting pellets made of the samples were placed in a flow cell and evacuated under reduced pressure at 693 K for 4 h. After cooling to room temperature, the samples were saturated with pyridine vapor and then evacuated at 473, 573, or 623 K for 30 min. Spectra were recorded at each evacuation temperature in the 4000–650  $\text{cm}^{-1}$  range by coaddition of 32 scans. The amount of Lewis acid sites in the samples was determined from the integral intensity of the characteristic band at *ca.* 1450  $\text{cm}^{-1}$  using the molar extinction coefficients from Emeis (2.22  $\text{cm} \mu\text{mol}^{-1}$ ).<sup>43</sup>

The surface areas and pore volumes of the calcined samples were measured by means of nitrogen adsorption at 77 K on a Quantachrome iQ-MP gas adsorption analyzer. Before the nitrogen adsorption, samples were dehydrated at 573 K for 6 h. The total surface area was calculated *via* the Brunauer–Emmett–Teller (BET) equation and the microporous pore volume was determined using the *t*-plot method. The mesopore size distribution was determined by the Barrett–Joyner–Halenda (BJH) method from the adsorption branches of the isotherms.<sup>25</sup>

Transmission electron microscopy (TEM) images of the samples were acquired on a Tecnai G2 F20 U-TWIN transmission electron microscope at an acceleration voltage of 200 kV. A few drops of the alcohol suspension containing the catalyst samples were placed on a micro grid, followed by evaporation at ambient temperature.

Diffuse reflectance ultraviolet-visible (UV-vis) spectra of the dehydrated samples were recorded against  $\text{BaSO}_4$  in the region of 200–700 nm on a Varian Cary 300 UV-vis spectrophotometer.

The  $^1\text{H}$  solid-state magic angle spinning nuclear magnetic resonance (MAS NMR) experiments were performed on a Bruker Avance III spectrometer at the resonance frequency of 400.1 MHz at a sample spinning rate of 8 kHz. The  $^1\text{H}$  MAS NMR spectra were recorded on the dehydrated samples, which were obtained by heating the samples at 673 K at a pressure below  $10^{-2}$  Pa for 12 h.

X-ray photoelectron spectra (XPS) of the dehydrated samples were recorded on a Kratos Axis Ultra DLD spectrometer with a monochromated  $\text{Al-K}\alpha$  X-ray source ( $h\nu = 1486.6$  eV), hybrid (magnetic/electrostatic) optics and a multi-channel plate and delay line detector (DLD). All spectra were recorded using an aperture slot of 300  $\times$  700 microns. Survey spectra were obtained with a pass energy of 160 eV and high-resolution spectra were obtained with a pass energy of 40 eV. Accurate binding energies ( $\pm 0.1$  eV) were determined with respect to the position of the adventitious C 1s peak at 284.8 eV.

#### 2.4 Catalytic evaluation

The catalytic investigations for aminolysis of epoxides were performed in a 25 mL round-bottom glass flask with a

cryogenic liquid condenser under atmospheric pressure. The vessel was charged with a mixture of equimolar quantities of the epoxide and amine (5 mmol), and 25 mg of the catalyst, and mixed vigorously using a magnetic stirrer. After the reaction, the mixture was monitored by taking out aliquots of the samples, diluting them with a known quantity of dichloromethane, separating the catalyst, and subjecting the diluted liquids to a Shimadzu GC 2010 (Agilent HP-5MS column, 30 m  $\times$  0.25 mm  $\times$  0.25  $\mu\text{m}$ ; FID detector). The GC peaks were identified by comparison with the retention times of the known standard samples, and by means of a Shimadzu GC-MS QP2010 SE equipped with an Agilent HP-5MS column.

To verify the potential recyclability of the Meso-Zr-Beta catalyst, recycling tests were performed. After each reaction completion, the mixture was centrifuged at 6000 rpm to deposit the solid catalyst, which was then washed with 5 mL of dichloromethane. After three repeated washing procedures, the catalyst sample was dried at 393 K overnight for the next reuse.

### 3. Results and discussion

#### 3.1 Evidence on the generation of intra-crystalline mesopores

In contrast to extensive reports on the introduction of mesopores into the ZSM-5 zeolite by alkaline treatment, very little is known about the behavior of Beta zeolite in NaOH solution.<sup>25–28</sup> Possible structural changes of the Beta zeolites after various post-treated procedures are investigated by X-ray diffraction and the corresponding powder patterns are shown in Fig. 1. Typical diffraction lines characteristic of the BEA topology are observed for the Meso-Beta samples compared with that of the corresponding counterpart H-Beta zeolite, confirming that the framework structure of Beta zeolites is well preserved after pre-dealumination and NaOH solution treatments

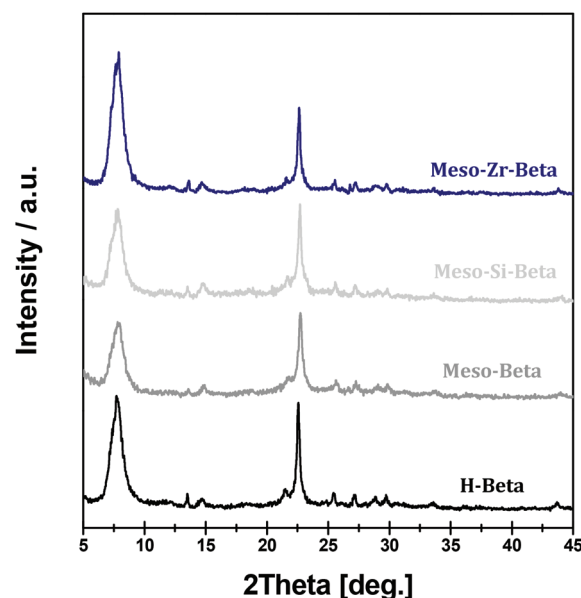


Fig. 1 XRD patterns of H-Beta and post-treated samples.

(no low angle XRD diffraction peak could be observed for all samples). Previous work has demonstrated that under a fixed desilication condition, the  $n_{\text{Si}}/n_{\text{Al}}$  ratio plays a crucial role in the formation of mesoporous zeolites and the optimal  $n_{\text{Si}}/n_{\text{Al}}$  for alkaline treatment strongly depends on the zeolite structure type.<sup>25,27,44,45</sup> Extensive research by Pérez-Ramírez *et al.*<sup>44,45</sup> verified that the optimal  $n_{\text{Si}}/n_{\text{Al}}$  ratio for creating mesoporous ZSM-5 is in the range of 25–50. However, if zeolite Beta with an  $n_{\text{Si}}/n_{\text{Al}}$  ratio of 35 was treated in a 0.2 mol L<sup>-1</sup> NaOH solution to generate hierarchically structured zeolites, a complete loss of crystallinity could be observed.<sup>25</sup> Compared with ZSM-5, the Beta zeolite is more susceptible to mesopore development when subjected to an alkaline treatment since the framework aluminum in the BEA framework is less stable.<sup>46</sup> The aluminum species will lose their function in controlling the selective extraction of silicon atoms and the corresponding mesopore generation by an alkaline treatment, if the  $n_{\text{Si}}/n_{\text{Al}}$  ratio is too high. In this study, the parent H-Beta zeolite ( $n_{\text{Si}}/n_{\text{Al}} = 16.7$ ) was pre-dealuminated to a reasonable  $n_{\text{Si}}/n_{\text{Al}}$  ratio of 22.4 and then subjected to alkaline treatment with a dilute NaOH solution (0.2 mol L<sup>-1</sup>) at 338 K for a short period of 0.5 h. It seems that zeolite Beta with a lower  $n_{\text{Si}}/n_{\text{Al}}$  ratio, *i.e.*  $n_{\text{Si}}/n_{\text{Al}} = 22$ , is more feasible for the formation of a hierarchical zeolite structure. On the other hand, after the incorporation of Zr species in the deep dealuminated Meso-Si-Beta sample *via* dry impregnation with Cp<sub>2</sub>ZrCl<sub>2</sub>, the Meso-Zr-Beta shows an identical XRD pattern, confirming the preservation of the Beta framework structure.

Fig. 2 depicts the N<sub>2</sub> adsorption–desorption isotherms of the H-Beta, Zr-Beta, and Meso-Zr-Beta samples. The Zr-Beta sample gives the same type I isotherm as the parent H-Beta zeolite, which is typical of microporous zeolites. These results are consistent with a previous report<sup>47</sup> that the dealumination procedure does not significantly change the structure of the zeolite and no mesopores could be generated. In contrast, a controlled alkaline treatment leads to the appearance of a distinct hysteresis loop at a relative pressure  $p/p_0$  of 0.4–0.8 for the Meso-Zr-Beta sample, showing a type IV isotherm, and gives substantial mesopore surface areas upon desilication (*vide infra*, Table 1). This indicates the presence of newly

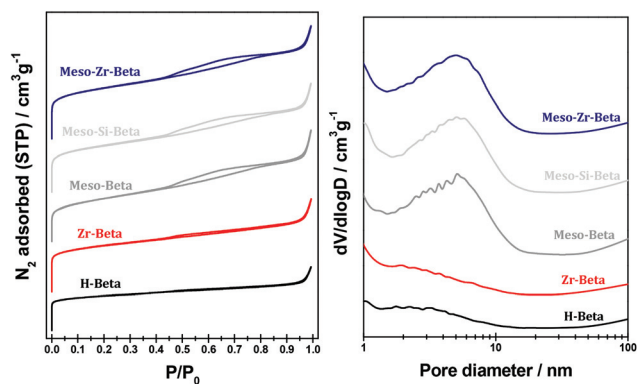


Fig. 2 N<sub>2</sub> adsorption and desorption isotherms (left) and pore size distribution (right) of H-Beta and post-treated samples.

Table 1 Physicochemical properties of parent H-Beta and post-treated samples

Sample	$n_{\text{Si}}/n_{\text{Al}}$ ratio <sup>a</sup>	$n_{\text{Si}}/n_{\text{M}}$ ratio <sup>a</sup>	SA (m <sup>2</sup> g <sup>-1</sup> )		PV (cm <sup>3</sup> g <sup>-1</sup> )	
			$S_{\text{BET}}$ <sup>b</sup>	$S_{\text{meso}}$	$V_{\text{micro}}$ <sup>c</sup>	$V_{\text{meso}}$
H-Beta	16.7	—	563	128	0.20	0.12
deAl-Beta	22.4	—	580	130	0.20	0.12
Meso-Beta	15.8	—	720	411	0.16	0.48
Meso-Si-Beta	>1800	—	745	420	0.17	0.52
Meso-Zr-Beta	>1800	97.0	720	425	0.16	0.50
Meso-Ti-Beta	>1800	97.2	730	418	0.16	0.49
Meso-Sn-Beta	>1800	96.8	731	420	0.17	0.50
Si-Beta	>1800	—	610	135	0.19	0.15
Zr-Beta	>1800	97.3	600	140	0.19	0.12
Ti-Beta	>1800	97.8	588	130	0.18	0.13
Sn-Beta	>1800	97.0	580	141	0.18	0.12

<sup>a</sup> Determined by ICP. <sup>b</sup> The specific surface area was obtained by the BET method. <sup>c</sup> Calculated from the  $t$ -plot.

created mesopores by the alkaline treatment, further evidenced by comparing the mesopore size distributions of the Zr-Beta and Meso-Zr-Beta samples using the BJH method (Fig. 2). In contrast to the Zr-Beta sample, Meso-Zr-Beta shows a pore distribution in the range of 2–10 nm and centered at *ca.* 5 nm, which is much smaller than the mesopore size observed for alkaline treated MFI<sup>44,45</sup> or MOR zeolites,<sup>21,48</sup> indicating the generation of smaller intra-crystalline mesopores in BEA zeolites.

The physicochemical properties of the parent H-Beta and post-treated samples are summarized in Table 1. The parent H-Beta sample possesses the typical micropore volume of 0.20 cm<sup>3</sup> g<sup>-1</sup> characteristic of the BEA topology, but with a higher mesopore surface area of 128 m<sup>2</sup> g<sup>-1</sup> than that of zeolite Beta synthesized *via* the fluoride route.<sup>25</sup> The latter is due to the contributions of a large amount of inter-particle voids originating from the disordered agglomeration of the small crystallites of the commercial zeolite Beta. It is generally accepted that the alkaline treatment results in desilication rather than dealumination of the zeolite framework.<sup>11,12,25,45,49</sup> Analysis results from ICP show that the  $n_{\text{Si}}/n_{\text{Al}}$  ratio of the Meso-Beta sample is lower than that of the partially dealuminated sample (deAl-Beta), confirming that predominantly silicon atoms have been removed from the framework of the Beta zeolite during the treatment in NaOH aqueous solutions. Meanwhile, the total surface area and the pore volume of mesopores increase after the alkaline treatment as a result of the mesopore formation. It should be noted that the concomitant decrease of the micropore volume from 0.20 cm<sup>3</sup> g<sup>-1</sup> for deAl-Beta to 0.16 cm<sup>3</sup> g<sup>-1</sup> for Meso-Beta may hint at the possibility of generating mesopores at the expense of destroying parts of the micropores. However, the amount of micropores consumed is far less than that of mesopores created. These results suggest that a large amount of mesopores is presumably generated in intra-crystal spaces, as clearly disclosed by TEM (*vide infra*, Fig. 3). As shown in Table 1, the desired  $n_{\text{Si}}/n_{\text{M}}$  ratios are also guaranteed in preparing (Meso-)Zr-Beta as well as (Meso-)Sn-Beta and (Meso-)Ti-Beta samples, confirming the high efficiency of the dry impregnation method.

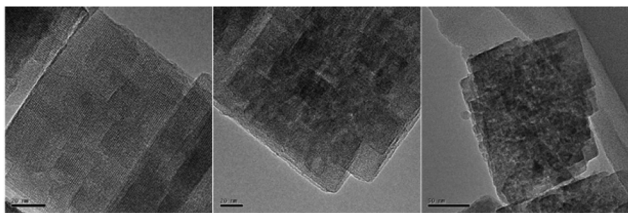


Fig. 3 TEM micrograph images of parent H-Beta (left), Zr-Beta (middle), and Meso-Zr-Beta (right).

TEM is further used to investigate the mesoporosity of these post-treated samples. Fig. 3 presents the TEM images of the Meso-Zr-Beta sample in comparison with H-Beta and Zr-Beta samples. Clearly, both H-Beta and Zr-Beta zeolites exhibit striped channels corresponding to the 12-MR micropores of Beta (Fig. 3, left and middle). These channels are arranged in a highly ordered manner without any interruption and almost free of unconnected regions. Hence, intra-crystal mesopores are hardly generated during the dealumination procedure *via* single acid treatment. In contrast, the alkaline treatment interrupts the continuity of the original micropore channels, making the newly formed mesopores visualized across the lattice planes. Accordingly, intra-crystalline mesopores exist randomly in a disordered pore size and shape throughout the whole crystals, as observed for the Meso-Zr-Beta zeolite (Fig. 3, right). On the other hand, it is generally accepted that silicon dissolution first occurs from the external surface area and subsequently progresses toward the center of the crystals.<sup>28</sup> This would shorten the diffusion pathway for the reactants diffusing from the outside into the micropores, maximize the mass transfer through the crystals, and finally improve the accessibility to the active sites located inside the pores.

### 3.2 Incorporation of Zr species into the zeolite framework

On the basis of our previous work,<sup>41,42</sup> Zr incorporation into the framework of mesoporous Beta was conducted *via* a post-synthesis strategy consisting of dealumination, desilication, and dry impregnation procedures, which involves the changes of silanol groups, which can be observed using infrared spectroscopy.

The FTIR spectra of the parent H-Beta and post-treated samples in the skeletal vibration region (700–1400  $\text{cm}^{-1}$ ) are shown in Fig. 4 (top). No obvious FTIR band in the range of 900–1000  $\text{cm}^{-1}$  can be observed for the H-Beta sample, while a band centered at *ca.* 953  $\text{cm}^{-1}$  occurs in the case of Meso-Beta, the intensity of which is exclusively enhanced by a further deep dealumination with a concentrated  $\text{HNO}_3$  solution to derive the Meso-Si-Beta sample. According to a literature report,<sup>50</sup> the newly formed band at *ca.* 953  $\text{cm}^{-1}$  should be due to the presence of a large amount of defect sites, as a consequence of framework atom extraction during the desilication and dealumination procedures in the present study. Subsequent dry impregnation with  $\text{Cp}_2\text{ZrCl}_2$  and calcination result in a noticeable decline of the IR band at *ca.* 953  $\text{cm}^{-1}$ , indicating an interaction between  $\text{Cp}_2\text{ZrCl}_2$  and defect sites. Mean-

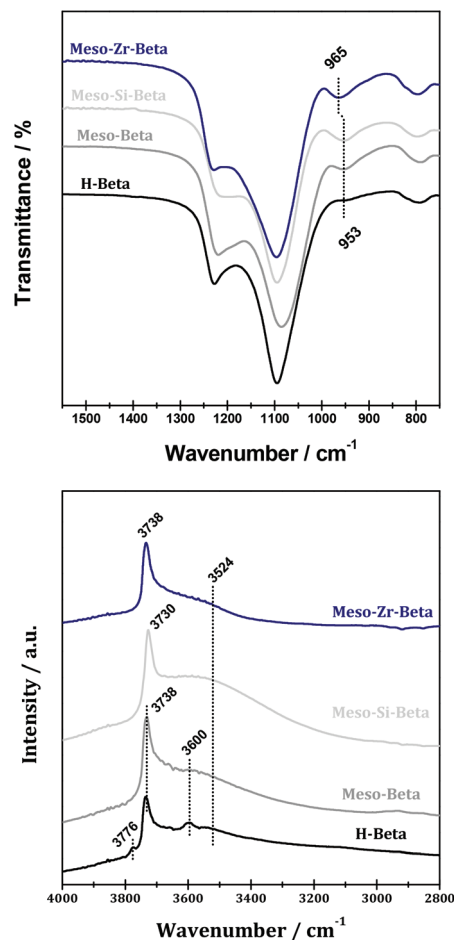


Fig. 4 FTIR spectra of the skeletal vibrations (top) and DRIFT spectra in the hydroxyl stretching vibration regions (bottom) of H-Beta and post-treated samples.

while, a new IR band centered at *ca.* 965  $\text{cm}^{-1}$  appears for the Meso-Zr-Beta sample, which is generally taken as an indication of metal incorporation into the zeolite framework and assigned to an asymmetric stretching mode of a  $[\text{SiO}_4]$  unit bonded to a  $\text{Zr}^{4+}$  ion ( $\text{O}_3\text{Si}-\text{O}-\text{Zr}$ ).<sup>40,51,52</sup>

The DRIFT spectra in the hydroxyl stretching region (3000–4000  $\text{cm}^{-1}$ ) of the parent H-Beta and post-treated samples are also presented (Fig. 4, bottom). The 3738  $\text{cm}^{-1}$  band of isolated terminal Si-OH groups, the 3600  $\text{cm}^{-1}$  band of bridging hydroxyl Si-OH-Al, the 3776  $\text{cm}^{-1}$  band of extra-framework Al-OH groups and the broad weak band of hydrogen-bonded Si-OH groups can be distinguished for parent H-Beta.<sup>53,54</sup> After treating with an oxalic acid solution, a new adsorption band at 3730  $\text{cm}^{-1}$  associated with a band due to isolated internal Si-OH at framework defects can be observed, while the characteristic bands of Al-OH species at 3776 and 3600  $\text{cm}^{-1}$  are preserved (not shown). This indicates that only a small quantity of Al species are eliminated by the pre-dealumination procedure in oxalic acid solution, in agreement with ICP analysis (the  $n_{\text{Si}}/n_{\text{Al}}$  ratio slightly increases from 16.7 to 22.4). The subsequent treatment of the partially dealuminated

Beta sample with a NaOH solution leads to a distinct increase in the intensity of the Si–OH band at  $3738\text{ cm}^{-1}$  due to terminal silanol associated with the enhanced external surface of the created mesopores through alkaline treatment.<sup>45,55</sup> In contrast to treatment with oxalic acid, the next dealumination procedure in a concentrated  $\text{HNO}_3$  solution results in the complete disappearance of the band at  $3776\text{ cm}^{-1}$ , evidencing the complete elimination of Al from the Meso-Beta zeolite framework ( $n_{\text{Si}}/n_{\text{Al}} > 1800$ ). Simultaneously, the intensification of the band at  $3730\text{ cm}^{-1}$  due to isolated internal Si–OH groups and the appearance of the band at  $3524\text{ cm}^{-1}$  related to hydrogen-bonded silanol groups are clearly observed, indicating the formation of defect sites at the vacant T-atom sites of the dealuminated Meso-Si-Beta framework. Dry impregnation of the obtained Meso-Si-Beta with the Zr precursor, *i.e.*  $\text{Cp}_2\text{ZrCl}_2$ , causes a decrease in the intensity of OH bands at  $3730$  and  $3524\text{ cm}^{-1}$ , suggesting that Zr species could react with silanols located in the vacant T-atom sites and thus be incorporated into the Meso-Beta zeolite framework.

In addition to infrared spectroscopy, solid state  $^1\text{H}$  MAS NMR spectra also give strong evidence on the evolution of hydroxyls during the Zr incorporation procedure. As shown in Fig. 5, a strong resonance signal at  $1.5\text{ ppm}$  due to silanol groups at framework defects and two weak resonance signals at  $2.5$  and  $3.9\text{ ppm}$  ascribed to extra-framework Al–OH groups and bridging hydroxyl Si–OH–Al,<sup>56</sup> respectively, can be clearly observed for the H-Beta sample. The combination of acid and alkaline treatment leads to the disappearance of hydroxyl groups associated with Al species responsible for resonance signals at  $2.5$  and  $3.9\text{ ppm}$ . On the other hand, the intensity of the signal at  $1.5\text{ ppm}$  due to the Si–OH group at framework defects increases strongly and a new broad resonance around  $2.7\text{ ppm}$  develops, indicating that additional framework defects covered with Si–OH groups are created during the acid

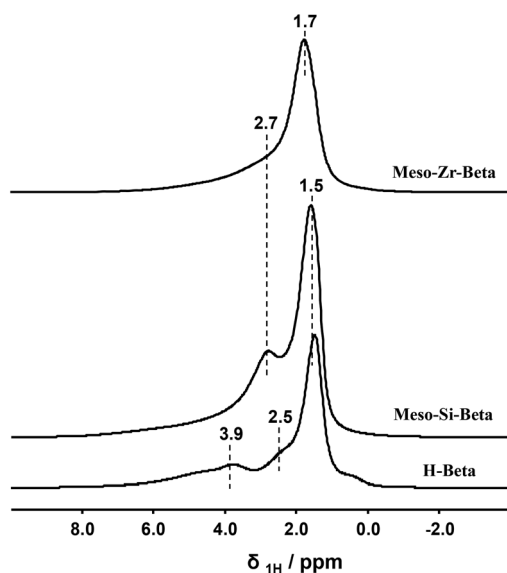
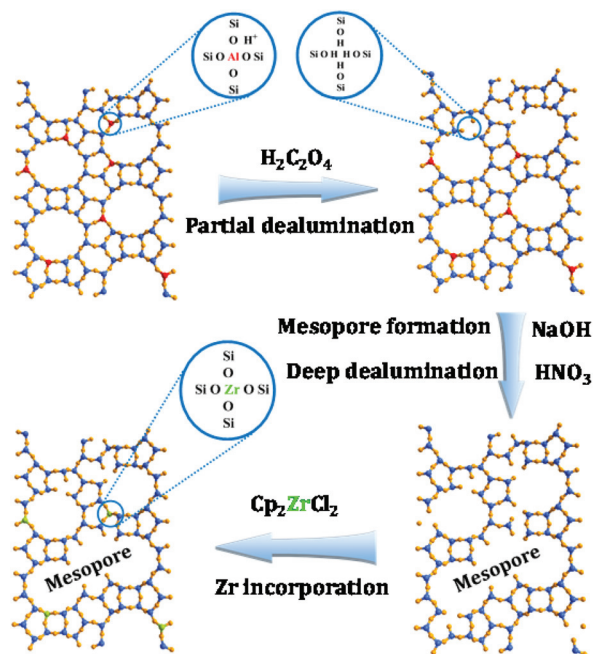


Fig. 5  $^1\text{H}$  MAS NMR spectra of H-Beta, Meso-Si-Beta, and Meso-Zr-Beta.



Scheme 1 Schematic representation of the intra-crystalline mesopore formation and tetrahedral Zr(IV) incorporation.

and alkaline treatment. The newly formed silanols causing the signal at  $2.7\text{ ppm}$  can be ascribed to Si–OH groups involved in hydrogen bonding to neighboring framework oxygen species inside the silanol nests, as described in our previous work.<sup>42</sup> The incorporation of Zr into the Meso-Si-Beta results in the disappearance of the silanol groups at framework defects and hydroxyl nests, leaving the remaining unreacted silanols with a chemical shift of  $1.7\text{ ppm}$ .

On the basis of results from infrared and solid-state  $^1\text{H}$  MAS NMR spectroscopy, the Meso-Zr-Beta sample could be prepared in a similar way to the Ti and Sn incorporation mechanism for preparing microporous Ti-Beta and Sn-Beta as reported in our previous work,<sup>41,42</sup> but involving an additional procedure to create mesopores prior to a deep dealumination step. The whole procedure employed in the post-synthesis of Meso-Zr-Beta, including partial dealumination, desilication, deep dealumination, and Zr incorporation, is illustrated in Scheme 1.

### 3.3 Existence states of Zr species in Meso-Zr-Beta

In order to evaluate the site isolation and the coordination states of the incorporated Zr species, diffuse reflectance UV-vis spectroscopy was first applied to the calcined samples. As shown in Fig. S1 (see ESI†), both Zr-Beta and Meso-Zr-Beta samples exhibit a strong absorbance band at *ca.*  $205\text{ nm}$ , which is ascribed to the charge-transfer transition between oxygen atoms and the metal centers. This band is generally accepted as the catalytically active Zr species in the framework with tetrahedral coordination.<sup>57–59</sup> It indicates that Zr species could be incorporated into the framework of BEA *via* the dry impregnation method and exist in a highly dispersed manner

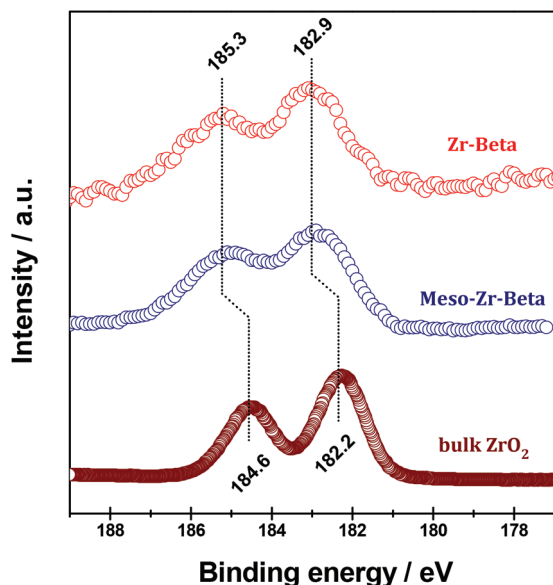


Fig. 6 Zr 3d XPS of Zr-Beta, Meso-Zr-Beta, and ZrO<sub>2</sub> samples.

(the contribution of very small and highly dispersed ZrO<sub>2</sub> nanoparticles cannot be fully excluded), in agreement with the results of FTIR spectroscopy.

The local environment of the Zr species in the dehydrated Zr-Beta and Meso-Zr-Beta samples was further studied by Zr 3d XPS. As shown in Fig. 6, the binding energy values of 182.9 and 185.3 eV corresponding to Zr 3d<sub>5/2</sub> and 3d<sub>3/2</sub>, respectively, could be observed for the two Zr-Beta samples, which are significantly higher than that of the bulk ZrO<sub>2</sub> reference (182.2 and 184.6 eV). This shift toward higher values should be due to the presence of Si–O–Zr bonds in the BEA structure and the change in geometry from octahedral to tetrahedral-coordination (*i.e.* formation of the tetrahedrally coordinated framework Zr species; the contribution of very small and highly dispersed ZrO<sub>2</sub> nanoparticles cannot be fully excluded), which is in accordance with the results of UV-vis spectroscopy. The higher binding energy of Zr 3d indicates a higher positive charge on Zr atoms incorporated into the silica framework due to the lower electronegativity of Zr than that of Si.<sup>6</sup> These observations are in good agreement with those reported for hydrothermally synthesized Zr-Beta zeolites<sup>5,6</sup> and post-synthesized Zr(IV)-containing MFI zeolites.<sup>51</sup>

### 3.4 Acidic properties of Meso-Zr-Beta

FTIR spectra of pyridine adsorption and desorption experiments are obtained in order to unravel the detailed information about the amount and strength of Lewis acid sites in Meso-Sn-Beta, Meso-Zr-Beta, and Meso-Ti-Beta samples, as shown in Fig. 7. No absorption bands can be observed for the Meso-Si-Beta sample since it is free of any Lewis acid sites. On the other hand, distinct bands at *ca.* 1445, 1490, and 1610 cm<sup>-1</sup> corresponding to the different vibration modes of the pyridine-rings adsorbed on the Lewis acid sites<sup>60,61</sup> could be observed for Meso-Me-Beta, evidencing the creation of

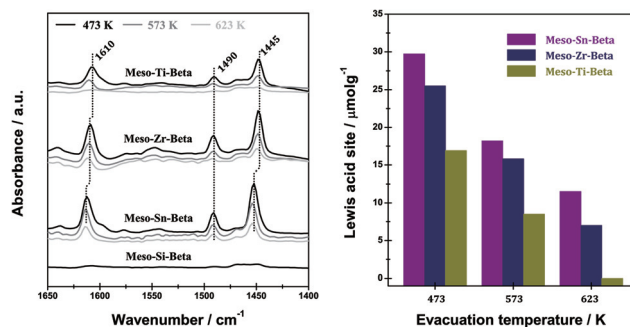
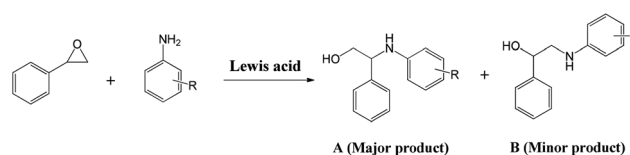


Fig. 7 FTIR spectra of Meso-Sn-Beta, Meso-Zr-Beta, and Meso-Ti-Beta samples (left) and their corresponding Lewis acid site densities (right) obtained from pyridine adsorption followed by evacuation at 473, 573 and 623 K.

Lewis acid sites upon the incorporation of transition metal ions. The pyridine adsorbed on Lewis acid sites could survive evacuation at high temperatures, *i.e.* 573 K for Meso-Ti-Beta, and 623 K for Meso-Sn-Beta and Meso-Zr-Beta, indicating the high strength of Lewis acid sites obtained. For a better comparison of the Lewis acid strength of samples, a quantitative analysis on the Lewis acid site densities measured by desorption of pyridine at various temperatures is carried out (Fig. 7, right). The Lewis acidity, including the density and strength, could be determined as Meso-Sn-Beta > Meso-Zr-Beta > Meso-Ti-Beta. This sequence coincides well with that observed for conventional microporous counterparts, *i.e.* Sn-Beta > Zr-Beta > Ti-Beta, reported in previous studies,<sup>41,62,63</sup> and also consistent with the theoretical predictions for double framework heteroatom substituted BEA zeolites although the sitting of framework heteroatoms in the zeolite may be different.<sup>64</sup>

### 3.5 Catalytic activity of Meso-Zr-Beta in the ring-opening epoxides with amines

The as-prepared solid Lewis acids are studied as catalysts in the ring-opening reaction of styrene oxide with aniline, in which two regio-isomer  $\beta$ -amino alcohol products, *i.e.* 2-phenyl-2-(phenylamino)ethanol and 1-phenyl-2-(phenylamino)ethanol, could be obtained (Scheme 2). Under our reaction conditions, the ring-opening reaction does not proceed without a catalyst and very little product (<3%) is obtained in the presence of H-Beta ( $n_{\text{Si}}/n_{\text{Al}} = 100$ ) as a catalyst, as shown in Table 2. Zr(IV)-containing Beta zeolites seem to be better catalysts, compared with Sn(IV)- and Ti(IV)-silicate analogues, with similar metal loadings, regardless of the presence of



Scheme 2 Ring-opening of epoxides with amines over a solid Lewis acid catalyst.

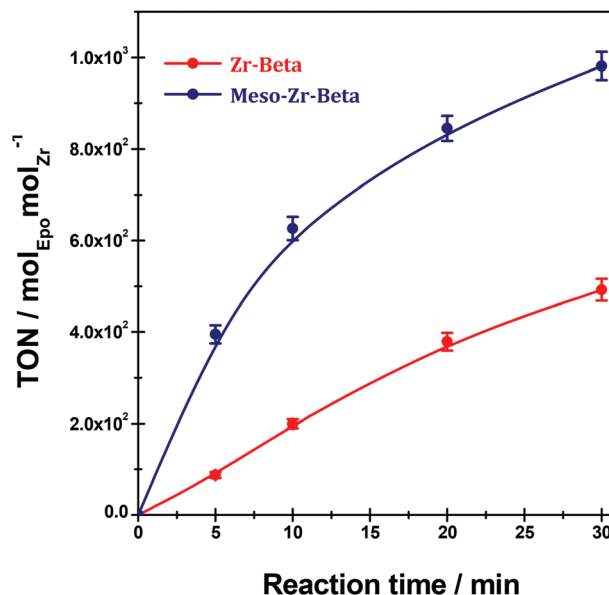
**Table 2** Aminolysis of styrene oxide with aniline over various zeolite catalysts<sup>a</sup>

Catalyst	Styrene oxide conv. (%)	$\beta$ -Amino alcohol select. (%)		TON <sup>b</sup> (mol <sub>Epo</sub> mol <sub>M</sub> <sup>-1</sup> )
		A	B	
H-Beta	<3%	—	—	—
Sn-Beta	25.4	91.0	9.0	305
Ti-Beta	35.5	92.8	7.2	417
Zr-Beta	40.5	94.4	5.6	473
Meso-Sn-Beta	41.0	91.1	8.9	476
Meso-Ti-Beta	56.6	92.4	7.6	660
Meso-Zr-Beta	80.7	94.7	5.3	939

<sup>a</sup> Reaction conditions: 5 mmol epoxide, 5 mmol amine, 25 mg catalyst, temperature = 308 K, reaction time = 0.5 h. <sup>b</sup> Calculated as the number of moles of styrene oxide converted per mole of the metal center.

mesopores or not. These results indicate that framework-incorporated Zr(IV) species are the optimized active components for the ring-opening reaction of epoxides with amines. On the other hand, the pore structure of zeolites is of great significance to the catalytic activity considering the mass transfer of bulky molecules during the reaction. The observed low activity of conventional Beta catalysts should be ascribed to their microporous structures with relatively small pores. With a hierarchical pore structure, mesoporous Beta materials possess larger surface areas and mesopore volumes (Table 1). The mesopores obtained from alkaline treatment are connected to the outer surface of the crystals and might be interconnected with the micropores as well. This unique structure provides a better accessibility of the reactant molecules to the active sites inside the pores and a facile diffusion of product molecules through mesopores, leading to an enhanced catalytic activity. For a better visualized understanding of the positive effect of newly created mesopores, the time-dependent specific activity per Zr site (TON) in Zr-Beta and Meso-Zr-Beta in the styrene oxide aminolysis reaction with aniline is calculated, as shown in Fig. 8. The TON values increase with prolonged reaction time over both Zr-Beta and Meso-Zr-Beta catalysts. Meso-Zr-Beta appears to be much more active than Zr-Beta with an initial TON over three times higher than the latter one. On the basis of catalytic results discussed above, we come to a conclusion that the highly active Lewis acid sites and the unhindered diffusion of reactants and products through catalyst crystals are two key factors controlling the ring-opening reaction of epoxides with amines over the modified Beta zeolites under study.

In order to broaden the substrate scope, the epoxide ring-opening reactions are investigated by varying the epoxide and amine reactants with optimized Meso-Zr-Beta as the catalyst. As shown in Table 3, a series of  $\beta$ -amino alcohols could be obtained with high regio-selectivity from the styrene oxide and different amines. The reactivity depends very much on the nature and type of amines used. Compared with aniline, substituted anilines afford lower yields of the products. On the other hand, the lowest yield of  $\beta$ -amino alcohols is produced

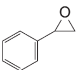
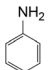
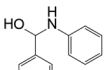
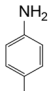
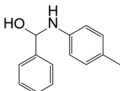
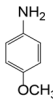
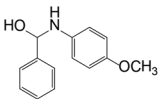
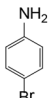
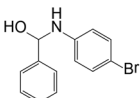
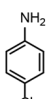
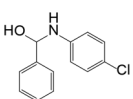
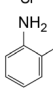
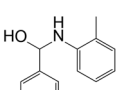
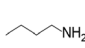
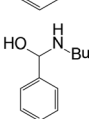
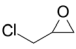
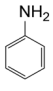
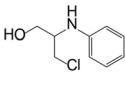
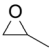
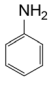
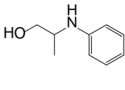


**Fig. 8** Time-dependent ring-opening aminolysis activity of Zr-Beta and Meso-Zr-Beta samples. Reaction conditions: 5 mmol epoxide, 5 mmol amine, 25 mg catalyst, temperature = 308 K.

when aliphatic primary, *i.e.* *n*-butylamine, is used instead of aniline. A similar trend in the catalytic activity has been observed using Ti-containing zeolites<sup>38,39</sup> or nanocrystalline Zr-MFI as catalysts.<sup>40</sup> The observed results could be illustrated according to the  $pK_a$  value, *i.e.* the basicity of amines, and the adsorption ability of reactant molecules. As depicted in Fig. 9, there is a good correlation between the aminolysis rate and  $pK_a$  values of the amines. With the increasing basicity of the amines, the reaction rate decreases accordingly for most of the amine substrates. Aminolysis of epoxides with amines is a bimolecular reaction,<sup>39</sup> in which both reactant molecules can absorb at the active sites. Hence, there should be an optimum bonding between the active sites of the catalyst and the reactant molecules. In this case, if amine molecules are strongly bonded to the Zr sites, the masked sites will not be available to activate epoxides for the ring-opening reaction. This is just the case using *n*-butylamine as the substrate, where the reaction cannot proceed smoothly due to the strong adsorption of the amine. As proposed in the literature,<sup>40</sup> the preferential adsorption of epoxides over amines is good for the reactivity of the ring-opening reaction. Epoxides are preferentially adsorbed and activated on the active sites, followed by attack of amines to result in a ring-opening to form  $\beta$ -amino alcohols. As shown in Table 3, the reactivity decreases in the sequence of styrene oxide > epichlorohydrin > propene oxide. This order may be ascribed to the higher epoxide/amine adsorption ratio for styrene oxide than the other two epoxides. On the basis of the facts discussed above, it would provide a reasonable explanation that zirconosilicates exhibit a higher activity than titanosilicates and stannosilicates. The Lewis acid strength of the three active sites is determined to be in the order Sn<sup>4+</sup> > Zr<sup>4+</sup> > Ti<sup>4+</sup>. Herein, we presume that amine molecules are strongly



Table 3 Ring-opening of epoxides with amines over the Meso-Zr-Beta catalyst<sup>a</sup>

Epoxide	Amine	$\beta$ -Amino alcohol	Epoxide conv. (%)	Select. (%)	TON <sup>b</sup> (mol <sub>Epo</sub> mol <sub>Zr</sub> <sup>-1</sup> )
			80.7	94.7	939
			52.2	92.5	608
			51.5	92.3	599
			75.0	97.5	873
			74.4	96.7	866
			60.3	95.1	702
			5.8	21.5	68
			74.4	95.8	866
			60.0	81.5	698

<sup>a</sup> Reaction conditions: 5 mmol epoxide, 5 mmol amine, 25 mg catalyst, temperature = 308 K, reaction time = 0.5 h. <sup>b</sup> Calculated as the number of moles of styrene oxide converted per mole of Zr.

bonded to the Sn<sup>4+</sup> sites due to their strong Lewis acidity, while Ti<sup>4+</sup> sites are not sufficient to adsorb and activate the epoxide substrate, both resulting in a stronger adsorption of aniline over styrene oxide. In contrast, Zr<sup>4+</sup> sites with moderate Lewis acidity appear to be the best candidates for the ring-opening epoxide reaction with amines (Table 2). To confirm our hypothesis, competitive adsorption experiments were carried out with the catalysts under study. The adsorption of both styrene oxide and aniline is estimated and compared with the catalytic activity obtained. As disclosed in Table 4, Meso-Zr-Beta, with the highest styrene oxide/aniline adsorption ratio of 1.45, exhibits the best catalytic performance with regard to styrene oxide conversion and aminolysis reaction rate, followed by Meso-Ti-Beta (1.33) and Meso-Sn-Beta (0.47). A direct comparison between the catalytic activity of the ring-opening aminolysis of styrene oxide with aniline (in terms of TON) over our catalysts and those reported in the literature is summarized in Table S1.†

It is well known that most of the reactions of epoxides involve the opening of the epoxide ring, including the addition of a proton to the epoxide oxygen and the deprotonated molecule of the substrate to one of the carbon atoms of the oxirane ring.<sup>65</sup> The ring-opening of epoxides can occur under neutral, basic or acidic conditions. Under acidic conditions, the addition of the nucleophile is considerably accelerated due to the reversible formation of the more reactive conjugate acid of the epoxide.<sup>39</sup> Here, tetrahedrally coordinated Zr(IV) species in the Beta framework act as Lewis acid centers in the epoxide ring-opening reaction, and the preferential adsorption and activation of epoxides on these active sites over amines is most crucial to form  $\beta$ -amino alcohols. In the case of styrene oxide as the epoxide substrate, the S<sub>N</sub>1 mechanism is more favorable and involves the polarization of the C–O bond to form a more stable carbocation from the epoxide (Scheme 3).

Compared with microporous zeolites, hierarchical/mesoporous materials cannot only significantly improve the catalytic

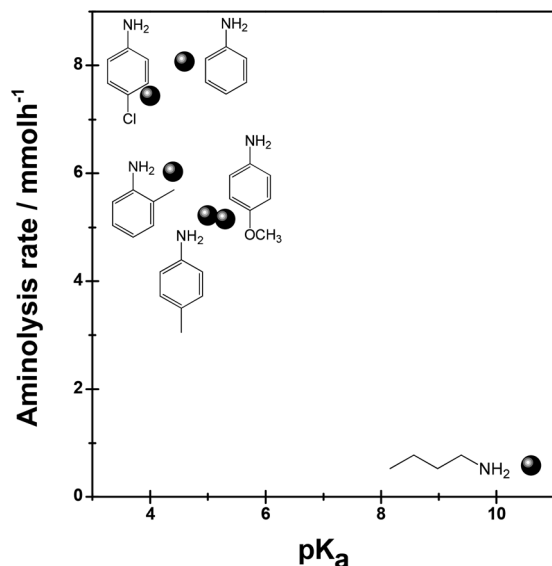


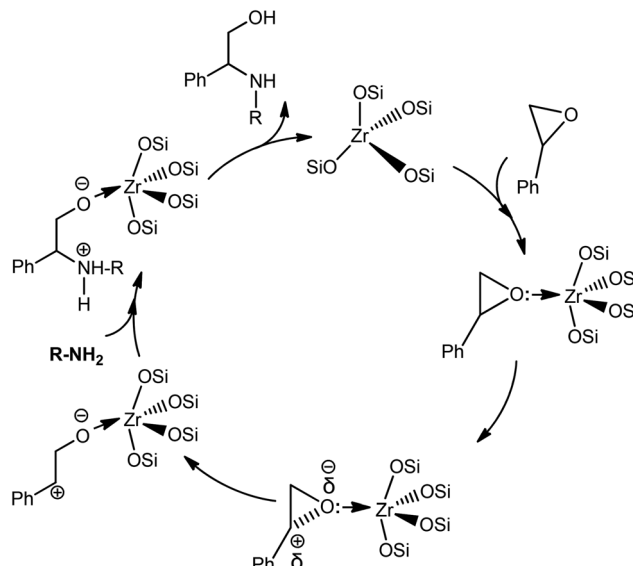
**Fig. 9** Correlation between the catalytic activity and the  $pK_a$  values of amines in the ring-opening aminolysis of styrene oxide. Reaction conditions: 5 mmol epoxide, 5 mmol amine, 25 mg catalyst, temperature = 308 K, reaction time = 0.5 h.

**Table 4** Competitive adsorption of styrene oxide and aniline on zeolite catalysts<sup>a</sup>

Catalyst	Substrate adsorbed (mmol $g_{zeolite}$ )		Epoxide/ amine ratio	Epoxide conv. <sup>b</sup> (%)	Aminolysis rate <sup>b</sup> (mmol $h^{-1}$ )
	Styrene oxide	Aniline			
Meso-Zr-Beta	0.16	0.11	1.45	55.1	5.5
Meso-Ti-Beta	0.12	0.09	1.33	38.0	3.8
Meso-Sn-Beta	0.08	0.17	0.47	29.5	3.0

<sup>a</sup> 100 mg of the zeolite was suspended for 0.5 h with equimolar amounts (2 mmol) of styrene oxide and aniline dissolved in 5 mL of  $CH_2Cl_2$ . Then, the catalyst was separated and the concentration of the substrate in the liquid portion was determined by gas chromatography. The amount adsorbed on the catalyst surface was determined by substrate concentration difference. <sup>b</sup> Epoxide conversion and aminolysis rate were obtained at 298 K after a reaction time of 0.5 h.

activities due to their enlarged pore openings and shorter diffusion pathways, but also can effectively suppress the catalytic deactivation when dealing with bulky reactants or products in the liquid phase due to their much higher external surface. The recycling abilities of Zr-Beta and Meso-Zr-Beta catalysts in the ring-opening reaction of styrene oxide with aniline are further examined. As shown in Fig. 10, significant catalytic deactivation occurred over the conventional Zr-Beta sample after only one cycle, while no obvious change in the catalytic aminolysis activity could be observed even after four successive recycling over Meso-Zr-Beta, confirming the vital role of mesopores against catalytic deactivation. The possible leaching of Zr species during the recycle experiments can be excluded by ICP analysis (Table S2<sup>†</sup>). XRD and surface area analyses rule out the possible change in the texture properties of the



**Scheme 3** Plausible mechanism for the ring-opening of styrene oxide with amines catalyzed by Meso-Zr-Beta.

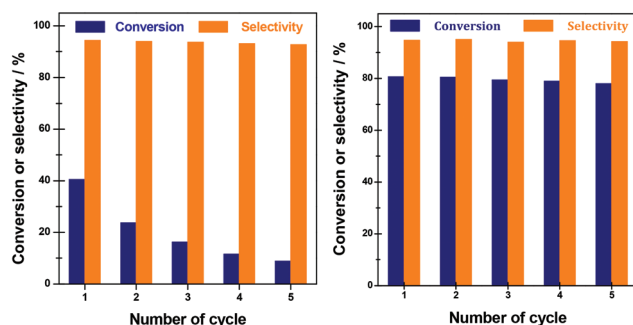


**Fig. 10** Recycling test for the ring-opening of styrene oxide with aniline over Zr-Beta (left) and Meso-Zr-Beta (right). Reaction conditions: 5 mmol epoxide, 5 mmol amine, 25 mg catalyst, temperature = 308 K, reaction time = 0.5 h.

Meso-Zr-Beta sample (Fig. S5 & Table S2<sup>†</sup>). The good recyclability of Meso-Zr-Beta demonstrates its great potential for future applications.

## 4. Conclusion

In this study, mesoporous BEA-type zirconosilicate has been successfully prepared *via* a post-synthesis strategy consisting of acid treatment, alkaline treatment, and dry impregnation with an organometallic Zr precursor. Briefly, a commercial H-Beta zeolite is treated in a dilute oxalic acid solution to obtain a partially dealuminated Beta sample, which is then subject to an alkaline treatment for framework desilication and the creation of intra-crystalline mesopores. The mesoporous Beta zeolite is treated in a concentrated nitric acid solution to derive siliceous Meso-Si-Beta, creating vacant T sites with associated silanol

groups. The organometallic Zr precursor  $\text{Cp}_2\text{ZrCl}_2$  can interact with vacant T sites in the Meso-Si-Beta and Zr species are subsequently incorporated into the framework of the mesoporous Beta zeolite upon calcination. The strategy developed here can be extended to the preparation of other mesoporous zeolites with incorporated transition metal ions.

The catalytic performance of mesoporous metal ion-containing Beta zeolites, *i.e.* Meso-Zr-Beta, Meso-Sn-Beta, and Meso-Ti-Beta, was investigated in the ring-opening reaction of styrene oxide with aniline for the selective production of 2-phenyl-2-(phenylamino)ethanol. Zr species in the BEA framework are evidenced to be optimized active components with moderate Lewis acidity for the aminolysis of epoxides, in comparison with Sn and Zr-silicate analogues. The mesopores generated by alkaline treatment enable better accessibility of reactant molecules to the active sites and more facile diffusion of products outside the pores, resulting in an enhanced catalytic activity. Through aminolysis of epoxides, a series of  $\beta$ -amino alcohols can be successfully synthesized by varying the epoxides and amines. The catalytic aminolysis rate is rationalized by the  $\text{p}K_{\text{a}}$  values of the amines used and the adsorption abilities of the reactant molecules. Meso-Zr-Beta, prepared by post-synthesis procedures, is demonstrated to be a robust catalyst in the ring-opening aminolysis of epoxides with good recyclability.

## Acknowledgements

This work was financially supported by the National Natural Science Foundation of China (21373119), the Ministry of Education of China (IRT13022, IRT13R30) and 111 Project (B12015). Furthermore, M.H. wants to acknowledge financial support by Deutsche Forschungsgemeinschaft.

## Notes and references

- 1 Y. Román-Leshkov and M. E. Davis, *ACS Catal.*, 2011, **1**, 1566.
- 2 H. J. Cho, C.-C. Chang and W. Fan, *Green Chem.*, 2014, **16**, 3428.
- 3 A. Corma, L. T. Nemeth, M. Renz and S. Valencia, *Nature*, 2001, **412**, 423.
- 4 M. S. Holm, S. Saravanamurugan and E. Taarning, *Science*, 2010, **328**, 602.
- 5 J. J. Pacheco and M. E. Davis, *Proc. Natl. Acad. Sci. U. S. A.*, 2014, **111**, 8363.
- 6 V. L. Sushkevich, I. I. Ivanova, S. Tolborg and E. Taarning, *J. Catal.*, 2014, **316**, 121.
- 7 L. Bui, H. Luo, W. R. Gunther and Y. Román-Leshkov, *Angew. Chem., Int. Ed.*, 2013, **52**, 8022.
- 8 T. De Baerdemaeker, B. Steenackers and D. De Vos, *Chem. Commun.*, 2013, **49**, 7474.
- 9 M. Moliner, *Dalton Trans.*, 2014, **43**, 4197.
- 10 A. Corma, *Chem. Rev.*, 1997, **97**, 2373.
- 11 J. Pérez-Ramírez, C. H. Christensen, K. Egeblad, C. H. Christensen and J. C. Groen, *Chem. Soc. Rev.*, 2008, **37**, 2530.
- 12 R. Chal, C. Gerardin, M. Bulut and S. van Donk, *ChemCatChem*, 2011, **3**, 67.
- 13 S. Lopez-Orozco, A. Inayat, A. Schwab, T. Selvam and W. Schwieger, *Adv. Mater.*, 2011, **23**, 2602.
- 14 K. M. Jinka, S. C. Lee, S. E. Park and R. V. Jasra, *Stud. Surf. Sci. Catal.*, 2008, **174**, 1187.
- 15 K. Na, C. Jo, J. Kim, W. Ahn and R. Ryoo, *ACS Catal.*, 2011, **1**, 901.
- 16 H. Y. Luo, L. Bui, W. R. Gunther, E. Min and Y. Román-Leshkov, *ACS Catal.*, 2012, **2**, 2695.
- 17 H. J. Cho, P. Dornath and W. Fan, *ACS Catal.*, 2014, **4**, 2029.
- 18 J. Pérez-Ramírez, S. Mitchell, D. Verboekend, M. Milina, N. L. Michels, F. Krumeich, N. Marti and M. Erdmann, *ChemCatChem*, 2011, **3**, 1731.
- 19 D. P. Serrano, J. M. Escola and P. Pizarro, *Chem. Soc. Rev.*, 2013, **42**, 4004.
- 20 V. Valtchev, G. Majano, S. Mintova and J. Pérez-Ramírez, *Chem. Soc. Rev.*, 2013, **42**, 263.
- 21 H. Xu, Y. T. Zhang, H. H. Wu, Y. M. Liu, X. H. Li, J. G. Jiang, M. Y. He and P. Wu, *J. Catal.*, 2011, **281**, 263.
- 22 P. Y. Dapsens, M. Menart, C. Mondelli and J. Pérez-Ramírez, *Green Chem.*, 2014, **16**, 589.
- 23 P. Y. Dapsens, C. Mondelli, B. Kusema, R. Verel and J. Pérez-Ramírez, *Green Chem.*, 2014, **16**, 1176.
- 24 P. Y. Dapsens, C. Mondelli, J. Jagielski, R. Hauert and J. Pérez-Ramírez, *Catal. Sci. Technol.*, 2014, **4**, 2302.
- 25 J. C. Groen, S. Abelló, L. A. Villaescusa and J. Pérez-Ramírez, *Microporous Mesoporous Mater.*, 2008, **114**, 93.
- 26 K. Cheng, J. C. Kang, S. W. Huang, Z. Y. You, Q. H. Zhang, J. S. Ding, W. Q. Hua, Y. C. Lou, W. P. Deng and Y. Wang, *ACS Catal.*, 2012, **2**, 441.
- 27 F. P. Tian, Y. H. Wu, Q. C. Shen, X. Li, Y. Y. Chen and C. G. Meng, *Microporous Mesoporous Mater.*, 2013, **173**, 129.
- 28 K. Tarach, K. Góra-Marek, J. Tekla, K. Brylewska, J. Datka, K. Mlekodaj, W. Makowski, M. C. Igualada López, J. Martínez Triguero and F. Rey, *J. Catal.*, 2014, **312**, 46.
- 29 O. Mitsunobu, in *Comprehensive organic synthesis*, ed. B. M. Trost and I. Fleming, Springer, New York, 1991, vol. 6, p. 88.
- 30 D. J. Ager, I. Prakash and D. R. Schaad, *Chem. Rev.*, 1996, **96**, 835.
- 31 E. J. Corey and F. Y. Zhang, *Angew. Chem., Int. Ed.*, 1999, **38**, 1931.
- 32 P. O'Brien, *Angew. Chem., Int. Ed.*, 1999, **38**, 326.
- 33 A. Procopio, M. Gaspari, M. Nardi, M. Oliverio and O. Rosati, *Tetrahedron Lett.*, 2008, **49**, 2289.
- 34 S. V. Malhotra, R. P. Andal and V. Kumar, *Synth. Commun.*, 2008, **38**, 4160.
- 35 M. J. Bhanushali, N. S. Nandurkar, M. D. Bhor and B. M. Bhanage, *Tetrahedron Lett.*, 2008, **49**, 3672.
- 36 M. Moghadam, S. Tangestaninejad, V. Mirkhani, I. Mohammadpoor-Baltork, S. Gorjipoor and P. Yazdani, *Synth. Commun.*, 2009, **39**, 552.
- 37 J. K. Satyarthi, L. Saikia, D. Srinivas and P. Ratnasamy, *Appl. Catal., A*, 2007, **330**, 145.

- 38 L. Saikia, J. K. Satyarthi, D. Srinivas and P. Ratnasamy, *J. Catal.*, 2007, **252**, 148.
- 39 A. Kumar and D. Srinivas, *J. Catal.*, 2012, **293**, 126.
- 40 R. Kore, R. Srivastava and B. Satpati, *ACS Catal.*, 2013, **3**, 2891.
- 41 B. Tang, W. Dai, G. Wu, N. Guan, L. Li and M. Hunger, *ACS Catal.*, 2014, **4**, 2801.
- 42 B. Tang, W. Dai, X. Sun, N. Guan, L. Li and M. Hunger, *Green Chem.*, 2014, **16**, 2281.
- 43 C. A. Emeis, *J. Catal.*, 1993, **141**, 347.
- 44 J. C. Groen, J. C. Jansen, J. A. Moulijn and J. Pérez-Ramírez, *J. Phys. Chem. B*, 2004, **108**, 13062.
- 45 J. C. Groen, L. A. A. Peffer, J. A. Moulijn and J. Pérez-Ramírez, *Chem. – Eur. J.*, 2005, **11**, 4983.
- 46 J. C. Groen, L. A. A. Peffer, J. A. Moulijn and J. Pérez-Ramírez, *Microporous Mesoporous Mater.*, 2004, **69**, 29.
- 47 S. Dzwigaj, Y. Millot, J.-M. Krafft, N. Popovych and P. Kyriienko, *J. Phys. Chem. C*, 2013, **117**, 12552.
- 48 J. C. Groen, T. Sano, J. A. Moulijn and J. Pérez-Ramírez, *J. Catal.*, 2007, **251**, 21.
- 49 D. Verboekend and J. Pérez-Ramírez, *Catal. Sci. Technol.*, 2011, **1**, 879.
- 50 G. G. Juttu and R. F. Lobo, *Catal. Lett.*, 1999, **62**, 99.
- 51 B. Rakshe, V. Ramaswamy, S. G. Hegde, R. Vetrivel and A. V. Ramaswamy, *Catal. Lett.*, 1997, **45**, 41.
- 52 R. Szostak, *Molecular Sieves: Principles of Synthesis and Identification*, Van Nostrand Reinhold, New York, 1989, p. 317.
- 53 J. P. Nogier, Y. Millot, P. P. Man, T. Shishido, M. Che and S. Dzwigaj, *J. Phys. Chem. C*, 2009, **113**, 4885.
- 54 L. Li and N. Guan, *Microporous Mesoporous Mater.*, 2009, **117**, 450.
- 55 J. Pérez-Ramírez, S. Abelló, A. Bonilla and J. C. Groen, *Adv. Funct. Mater.*, 2009, **19**, 164.
- 56 M. Hunger, S. Ernst, S. Steuernagel and J. Weitkamp, *Microporous Mater.*, 1996, **6**, 349.
- 57 M. S. Morey, G. D. Stucky, S. Schwarz and M. Fröba, *J. Phys. Chem. B*, 1999, **103**, 2037.
- 58 J. E. Haskouri, S. Cabrera, C. Guillem, J. Latorre, A. Beltrán, B. Beltrán, M. D. Marcos and P. Amorós, *Chem. Mater.*, 2002, **14**, 5015.
- 59 A. Ramanathan, M. C. C. Villalobos, C. Kwakernaak, S. Telalovic and U. Hanefeld, *Chem. – Eur. J.*, 2008, **14**, 961.
- 60 R. Buzzoni, S. Bordiga, G. Ricchiardi, C. Lamberti, A. Zecchina and G. Bellussi, *Langmuir*, 1996, **12**, 930.
- 61 P. Li, G. Q. Liu, H. H. Wu, Y. M. Liu, J. G. Jiang and P. Wu, *J. Phys. Chem. C*, 2011, **115**, 3663.
- 62 A. Corma, M. E. Domine, L. Nemeth and S. Valencia, *J. Am. Chem. Soc.*, 2002, **124**, 3194.
- 63 A. Corma, M. E. Domine and S. Valencia, *J. Catal.*, 2003, **215**, 294.
- 64 G. Yang, E. A. Pidko and E. J. M. Hensen, *J. Phys. Chem. C*, 2013, **117**, 3976.
- 65 R. E. Parker and N. S. Isaacs, *Chem. Rev.*, 1959, **59**, 737.